

Squirrel-Cage Type Induction Machine Utilizing Space Harmonics for Secondary Excitation with Concentrated Winding Stator

Masahiro Aoyama / IEEE Member
Department of Electrical and Electronics Engineering
Shizuoka University
3-5-1 Johoku, Naka-ku, Hamamatsu, Shizuoka JAPAN
aoyama.masahiro@shizuoka.ac.jp

Toshihiko Noguchi / IEEE Senior Member
Department of Electrical and Electronics Engineering
Shizuoka University
3-5-1 Johoku, Naka-ku, Hamamatsu, Shizuoka JAPAN
noguchi.toshihiko@shizuoka.ac.jp

Abstract—This paper describes a novel squirrel cage type induction machine utilizing space harmonics for brushless secondary excitation. The unique point of this proposed technique is able to utilize space harmonic for additional torque generation. Its space harmonic is inevitably generated by concentrated winding structure. The magnetic circuit topology of brushless secondary excitation technique with space harmonic and its effects on torque increase is conducted by FE-analysis. Then, the driving performance are analytically revealed by comparing with conventional squirrel cage type induction machine.

Keywords—induction machine, concentrated winding stator, space harmonic, second excitation, multiple squirrel cage

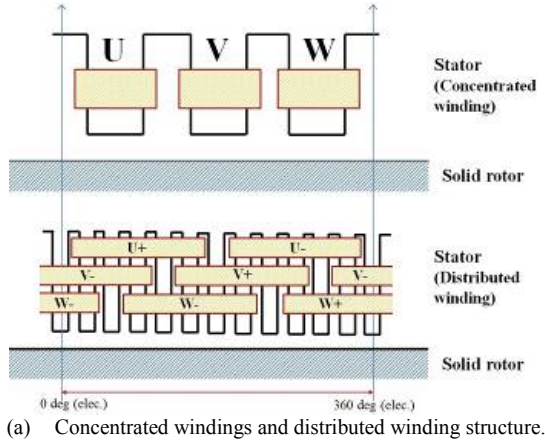
I. INTRODUCTION

In recent years, as an effort in the industrial society to reduce the burden on the global environment, it is strongly required to improve the efficiency of motors that convert electric energy into mechanical energy. A permanent magnet synchronous motor (PMSM), a wound-field synchronous motor (WFSM), and an induction motor (IM) can be cited as an example of a motor driving three phases. Especially, PMSM has features such as high torque density and high efficiency, but in the case of type using a neodymium magnet, it has resource procurement risk and risk of price fluctuation due to uneven distribution of production area. In addition, in the extremely low load region, the efficiency drops due to the iron loss caused by the magnetic flux of the permanent magnets (PMs), and the iron loss due to the flux weakening control becomes a problem in the high rotation region. In order to solve these problems, researches on variable magnetic flux technique, which makes the amount of magnetic flux linking to the armature winding variable without flux weakening control, are actively studied in recent years [1-11]. Various methods, such as variable magnet magnetism or variable skew structure, have been proposed for these techniques, but it is hard to say that any of the methods has reached the performance that exceeds the flux weakening control in terms of cost and motor performance.

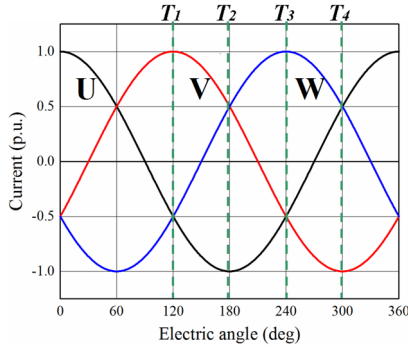
On the other hand, the IM that is conventional classical technique can be regarded as a kind of variable field motor based on its driving principle. Research on high torque and high efficiency of the IM has been studied in the past in various ways, but as far as the authors know, no research has been done on approaches that greatly change that structure. In terms of high performance by secondary excitation (doubly fed), it can be mentioned a method using classical slip-ring or brushless secondary excitation by rotating magnetic field of two kinds of frequencies (multiple rotating magnetic field

with nested-loop structure rotor) [12-15]. Since the former has slip-ring, problems remain in terms of maintainability and robustness, and the latter has the problem of requiring two inverters for variable speed driving and enlarging the motor size. On the other hand, as a conservative approach compared with the secondary excitation, reduction of the conductor eddy current loss due to the space harmonics have been reported by various approaches [16-20]. For example, the efforts to optimize the shape of the rotor slot in order to reduce harmonic secondary copper loss due to slot harmonic interlinking in the vicinity of the rotor gap, or the optimization of the gap length to reduce the carrier loss of IM driven by the PWM inverter (loss due to carrier harmonics in the stator, rotor core and conductor). In the data compiled by the Ministry of Economy, Trade and Industry of Japan in 2013, as an example, of the loss composition of the IM, the primary copper loss (the armature copper loss) is about 40 %, which is a large proportion of the previous loss. Research on an IM with a concentrated winding stator structure has been reported for the purpose of reducing primary copper loss so as to support these data [16,21]. By adopting a concentrated winding stator structure, the merit of the miniaturization by the shortening of the coil end space is increased particularly in a motor having a large space restriction when mounted on a vehicle as in electric car (EV) applications. However, the IMs with three-phase concentrated winding stator structure are hardly seen in the market. In the concentrated winding stator, a secondary space harmonic which rotates in opposite phase to the fundamental rotating magnetic field is generated, and its amplitude reaches about 50 % of the fundamental wave component. In the case of a synchronous motor, this asynchronously rotating space harmonic is consumed as the iron loss. On the other hand, in the case of the asynchronous motor, since the induced electromotive force is obtained on the rotor side by the slip, it becomes a complicated phenomenon in terms of driving principle. Even with space harmonics, induced electromotive force is generated on the rotor side and the harmonic secondary copper loss occurs. In other words, it is necessary to design not only slip against fundamental wave rotating magnetic field but also magnetic circuit design considering slip against harmonic rotating magnetic field.

In view of the above problems, this paper proposes a brushless secondary excitation technique that can also use the space harmonic for torque generation. Verify the effect of brushless secondary excitation by space harmonics by explaining the driving principle, structure design of the downsized prototype and its electromagnetic field analysis. Most of the conventional techniques reduce inductive electromotive force generated due to the space harmonics. However, this research is characterized by positively utilizing



(a) Concentrated windings and distributed winding structure.



(b) Three-phase armature currents.

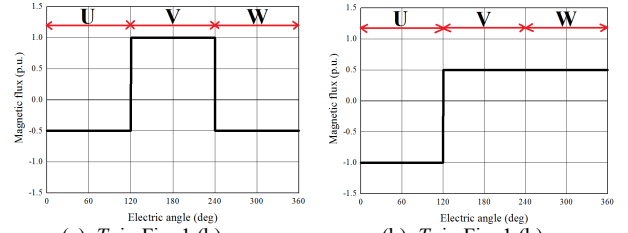
Fig. 1. Simplified armature winding structure and each time of armature current waveform.

space harmonic to generate torque by devising a special squirrel-cage rotor design, and it can be thought of an application of brushless doubly fed technique using a nested-loop rotor. That is, instead of generating passively different two types of rotating magnetic fields as in the prior technique, brushless doubly fed is realized by using two kinds of different rotating magnetic field inevitably generated in a concentrated winding stator structure.

II. DESIGN CONCEPT OF MAGNETIC CIRCUIT

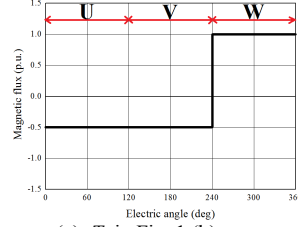
A. Distribution of Armature Magnetomotive Force of Concentrated Windings Stator

Figure 1 shows a simplified stator structure and three-phase stator current. Figure 2 shows the simplified gap magnetomotive force waveforms at each time (T_1 to T_4) in Fig. 1 (b). Figure 3 shows the waveform of the gap magnetomotive force obtained by approximating the waveform of Fig. 2 with only the fundamental wave and the secondary space harmonic [22]. From the Fig. 3, it can be confirmed that the second space harmonic proceeds in the opposite direction with respect to the fundamental wave as time goes on. From this, it can be said that the rotating magnetic field of two different frequencies are inevitably generated structurally in the concentrated winding stator. In other words, when the induction rotor is included in the concentrated winding stator, it is necessary to consider the slip s_1 with respect to the fundamental wave rotating magnetic field and the slip s_2 with respect to the second order space harmonic. Assuming that the rotation speed of the fundamental wave rotating magnetic field is N_s , the second order space harmonic is $2N_s$, and the rotation speed of the rotor is N_r , s_1 and s_2 are as follows.



(a) T_1 in Fig. 1 (b).

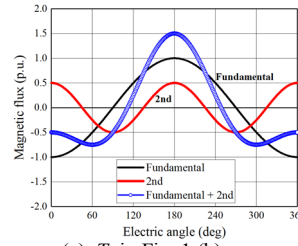
(b) T_2 in Fig. 1 (b).



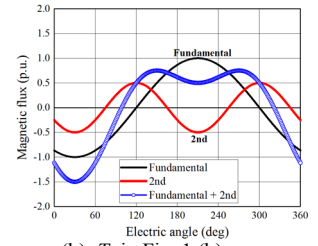
(c) T_3 in Fig. 1 (b).

(d) T_4 in Fig. 1 (b).

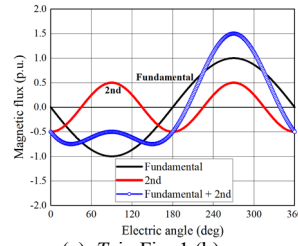
Fig. 2. Simplified magnetomotive force distribution without slot-opening harmonic in air-gap with respect to each time of current waveform.



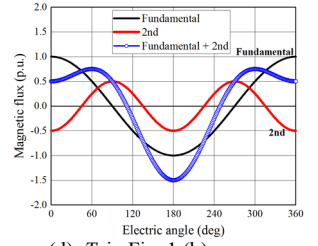
(a) T_1 in Fig. 1 (b).



(b) T_2 in Fig. 1 (b).



(c) T_3 in Fig. 1 (b).



(d) T_4 in Fig. 1 (b).

Fig. 3. Magnetomotive force distribution of Fig. 2 approximated by fundamental waveform and second-order space harmonic.

$$s_1 = \frac{N_s - N_r}{N_s}, \quad s_2 = \frac{2N_s - (-N_r)}{2N_s} = \frac{2N_s + N_r}{2N_s} \quad (1)$$

B. Special Squirrel-Cage Rotor Structure

When the rotor rotates synchronously ($N_r = N_s$), $s_1 = 0$ and $s_2 = 1.5$ from Eq. (1). Here, s_2 is based on the second order space harmonic as shown in Eq. (1), but when the fundamental wave is used as the reference, the slip of the second order space harmonic with respect to the fundamental wave is 3.0. As a result, when designing the magnetic circuit of the rotor with a general squirrel cage structure, the induced electromotive force of the third harmonic is generated by observing from the fundamental rotational coordinate during synchronization with the fundamental rotating magnetic field ($s_1 = 0$) due to s_2 . In order to solve the above problem, as shown in Fig. 4, the special squirrel-cage structure having two kinds, a rotor bar “Bar1” (“For fundamental” in Fig. 4) coupled to the fundamental wave rotating magnetic field and a rotor bar “Bar2” (“For space harmonic” in Fig. 4) coupling

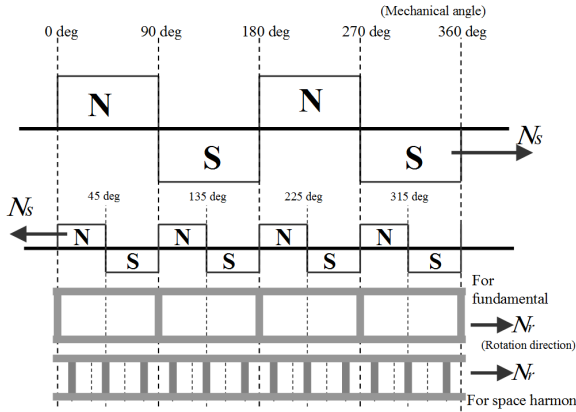


Fig. 4. Armature magnetomotive force and squirrel cage rotor design concept.

with the second order space harmonic are proposed in this paper. The Bar1 and the Bar2 are respectively short-circuited with end-rings, and the two kinds of rotor bars are constructed in an electrically independent state. That is, the proposed motor is composed of a plurality of squirrel cage type like the nested-loop type rotor. Here, Fig. 4 shows the case of a 4-pole structure as an example. In order to magnetically link Bar1 only to the fundamental wave, the rotor bars are arranged with a pitch of one pole, and a total of four rotor bars are short-circuited with end-rings. The Bar1 has a pitch corresponding to one pole pair of the second order space harmonic even if the second space harmonic wave interlinks, so that the magnetic interference due to the second space harmonic can be neglected. On the other hand, since the second space harmonic in the stationary coordinate is the magnetic field rotating in the reverse direction with respect to the fundamental wave, as described above, when observed on the fundamental synchronous rotation coordinate, it becomes the third order time harmonic. Therefore, Bar2 short-circuits 12 rotor bars in total with the end-ring. Here, due to the design of the rotor bar pitch, Bar2 has a low magnetic coupling coefficient, but induced electromotive force is generated when the fundamental wave rotating magnetic field interlinks. Furthermore, since the second space harmonic is about 0.5 times the amplitude with respect to the fundamental wave amplitude, it is necessary to adjust the slip s_2 - torque τ_2 characteristic with respect to s_1 by adjusting the secondary resistance R_{2-2} of Bar2. Here, τ_2 is the torque generated by the second space harmonic. Figure 3 shows s_1 - τ_1 characteristics for s_1 and s_2 - τ_2 characteristics for s_2 using IM torque equation derived from the general L-type equivalent circuit of Eq. (2).

$$\tau_{n(n=1,2)} = \frac{3V_1^2}{\omega_{n(n=1,2)}} \cdot \frac{\frac{R_2}{s}}{\left(R_1 + \frac{R_2}{s}\right)^2 + (X_1 + X_2)^2} \quad (2)$$

Here, V_1 is the applied voltage for one phase, R_1 and R_2 are the resistance of the stator and the rotor, and X_1 and X_2 is the reactance of the stator and the rotor, respectively. In order to understand the characteristics, Fig. 5 was calculated using appropriate motor parameters. In the Bar2, desk calculation was performed in which induced electromotive force was not generated by the fundamental wave rotating magnetic field, that is, approximate to that without magnetic interference by the fundamental rotating magnetic field. From this figure, it can be seen that the maximum torque ($\tau_1 + \tau_2$) can be

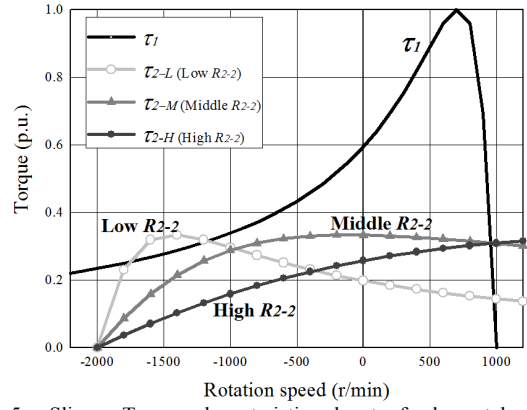
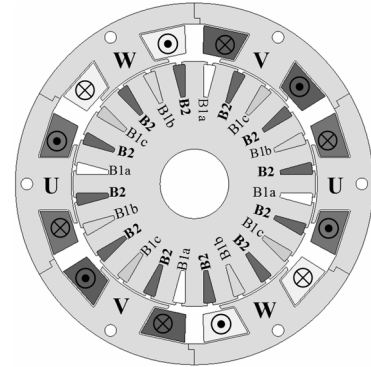
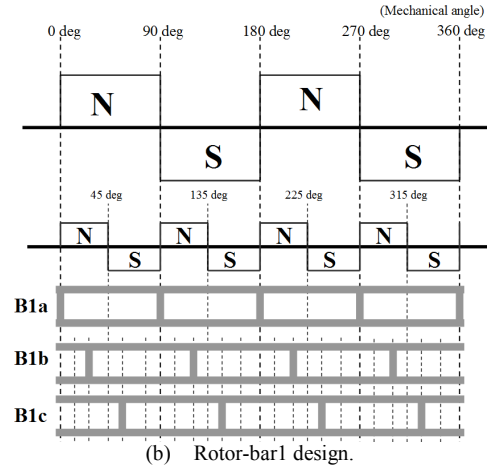


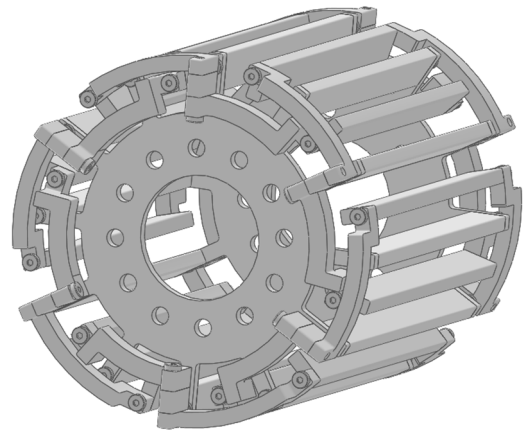
Fig. 5. Slip-vs.-Torque characteristics due to fundamental rotating magnetic field and Slip-vs.-Torque characteristics due to 2nd-order space harmonic. (Desk calculation with general motor parameter)



(a) Cross section diagram of proposed motor.



(b) Rotor-bar1 design.



(c) Rotor bar design.

(End-ring of rotor bar coupling to fundamental wave is not shown.)
Fig. 6. Downsized prototype for principle verification.

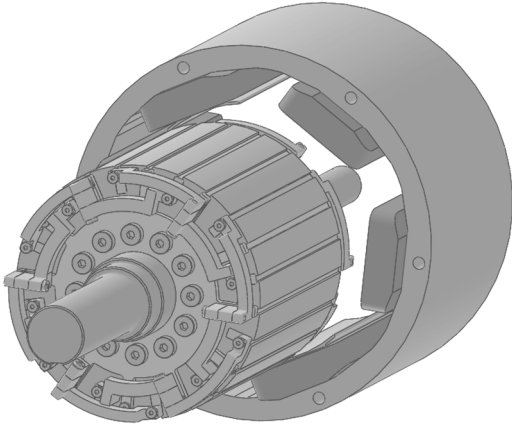


Fig. 7. Mechanical design of prototype.

improved by designing the secondary resistance R_{2-2} of Bar2 to be higher.

III. PERFORMANCE PREDICTION BY ELECTROMAGNETIC FIELD ANALYSIS

A. Miniaturized Principle Verification Machine

Figure 6 shows the cross-sectional view and structural design of the principle verification machine, and main specifications of prototype are shown in Table I. For the convenience of the notation space in this figure, the Bar1 is described as B1 and the Bar2 as B2. In anticipation of actual verification of the brushless doubly fed principle by space harmonic, magnetic circuit design is carried out with a miniaturized model of about 1 kW. As shown in Fig. 6, Bar1 to be coupled to the fundamental wave has a three-phase configuration by disposing B1a, B1b, B1c at 120 degrees in an electrical angle. In order to verify the actual machine in the case of three kinds of general squirrel-cage rotor structure in which all rotor bars are short-circuited, the squirrel-cage rotor structure without Bar2 for the space harmonics, and proposed motor, the rotor bar is designed to be detachable as shown in Fig. 7. Specifically, it is the structure in which the bar and the end-ring are fastened with bolts by cutting out from an aluminum conductor. As the electromagnetic steel plate of the stator core and rotor core, 35A230 material manufactured by Nippon Steel Sumitomo Metals is used.

B. Performance Prediction by FE-Analysis

Performance prediction by electromagnetic field analysis was carried out by two-dimensional electromagnetic field analysis using JMAG-Designer (ver. 16) developed by JSOL Corporation. Figure 8 shows the slip s_l – torque ($\tau_1 + \tau_2$) characteristic when the fundamental wave rotating magnetic field is 1000 r/min. The “Without B2” in this figure is the result when Bar2 is opened without short-circuiting with the end-ring. According to the figure, in the absence of Bar2, that is, no induced electromotive force is obtained by the second space harmonic, torque is greatly reduced when torque is generated only by the fundamental wave rotating magnetic field. Figure 9 shows the case where the end-ring of Bar1 is opened (Without B1), the case where the end-ring of Bar2 is opened (Without B2), and the sum of analysis results (Without B1 + Without B2) of the two cases. From this figure, it can be confirmed the result of “Without B1” the torque τ_2 generated by the second space harmonic and from the result of “Without B2” it can be confirmed that the torque τ_1 generated by the

Table I. Specifications of prototype.

| | |
|-------------------------------------|------------------------------|
| Number of poles and slots of stator | 4 pole, 6slots |
| Stator diameter and stack length | $\phi 125 \times L80$ |
| Number of rotor slots | 24 slots |
| Armature winding resistance | 1.0 Ω |
| Bar1 end-ring resistance | $1.07 \times 10^{-4} \Omega$ |
| Bar2 end-ring resistance | $0.98 \times 10^{-2} \Omega$ |
| Number of armature coil-turn | 110 |

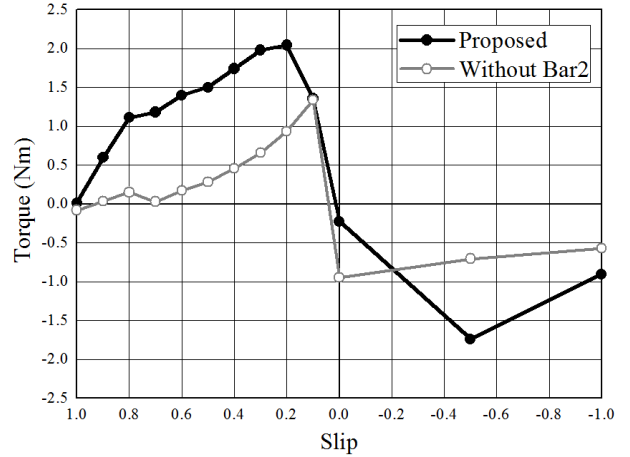


Fig. 8. Slip-vs.-torque characteristics. (Fundamental rotating magnetic field: 1000 r/min)

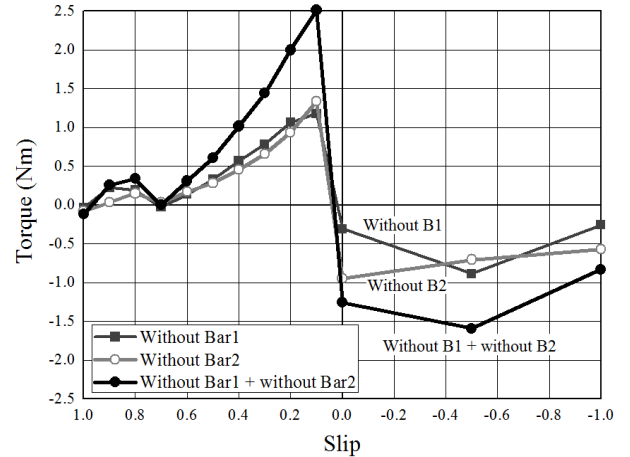


Fig. 9. Slip-vs.-torque characteristics without B1 or B2. (Fundamental rotating magnetic field: 1000 r/min)

fundamental wave is obtained. However, when comparing the result of “Proposed” of Fig. 8 with the result of “Without B1 + Without B2” of Fig. 9, the slip – torque characteristics are different. This is because the magnetic paths of the secondary magnetic flux generated by the induced current flowing in B1 and the secondary magnetic flux generated by the induced current flowing in B2 overlap each other as shown in Fig. 6, so that the inductance changes due to the interaction. Figure 10 shows the results of analyzing the slip s_l – torque characteristics under the same driving conditions as in Fig. 8 with the conventional squirrel-cage rotor bar structure (the rotor bar 6(a) is all short-circuited with the end-ring). The resistance of the end-ring is $1.07 \times 10^{-5} \Omega$. Figure 11 shows the induced current of the rotor bar ($s_l = 0.2$ as an example). From the Fig. 10 and Fig. 11, induced electromotive force of the harmonic is generated by the second space harmonic, and the rotor harmonic current is generated, and the torque is

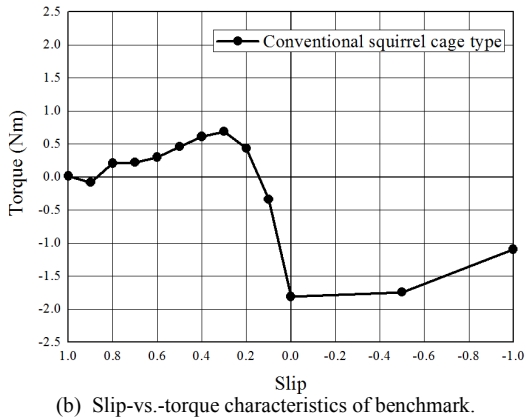
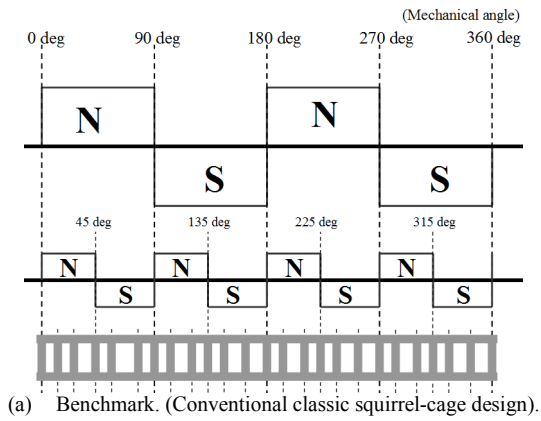


Fig. 10. Slip-vs.-torque characteristics at fundamental rotating magnetic field: 1000 r/min.

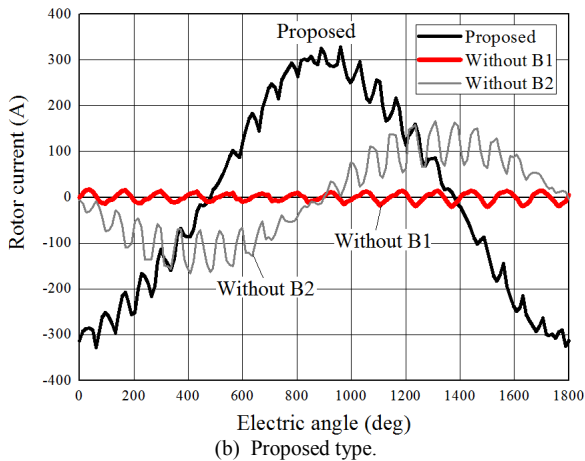
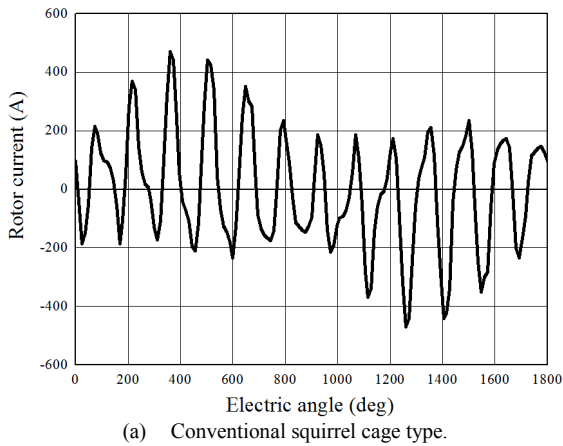


Fig. 11. Rotor current in rotor-bar conductor under slip $s_f = 0.2$.

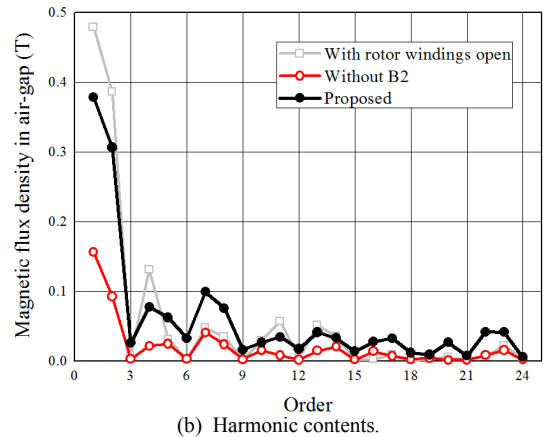
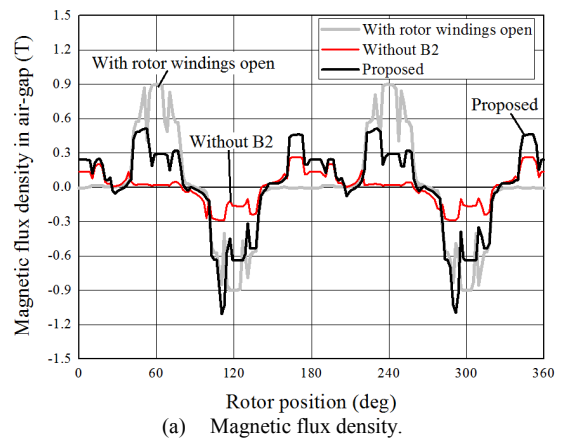
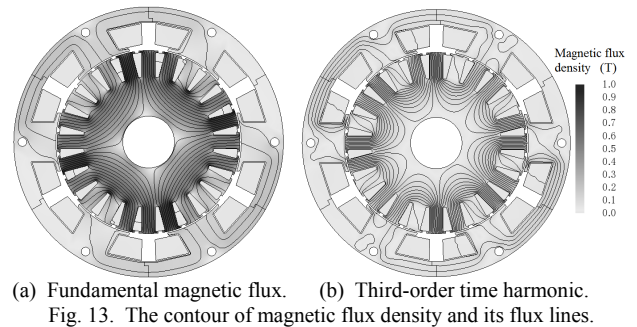


Fig. 12. Magnetic flux density in air-gap and its harmonic contents under slip $s_f = 0.2$.



reduced as the result. On the other hand, in the case of the proposed motor, as shown in Fig. 12, it can be confirmed that the harmonic components superimposed on the rotor current can be greatly reduced. Comparing with “Without B2” and “Proposed”, it is possible to reduce the rotor harmonic current by having B2. The secondary magnetic flux is generated at Bar2 by obtaining the induced electromotive force from the second space harmonic, but the secondary magnetic flux generated at Bar2 causes a change in inductance, which is considered to affect Bar1. As shown in Fig. 12, it can be confirmed that the secondary magnetic flux generated by Bar2 is magnetically interfered with Bar1 even when the gap magnetic flux waveform greatly changes by Bar2 when evaluated by the gap magnetic flux density. Further factor analysis needs to be done in the future. Figure 13 (a) shows the fundamental magnetic flux line magnetically coupled to Bar1, and Fig. 13 (b) shows a third-order time harmonic (observed on rotor coordinates) serving as a magnetomotive force source of Bar2. From the result of visualization of the magnetic flux lines, it can be said that the proposed motor is

brushless secondary excited by the third time harmonic in Bar2 and can be utilized for the torque generation.

IV. CONCLUSION

This paper proposed the novel brushless doubly-fed technique utilizing space harmonic, which is inevitably generated by the concentrated winding stator. The principle of second space harmonic inevitably occurring in a concentrated winding stator structure is described and the idea of a special squirrel-cage structure for generating torque by the secondary excitation with second space harmonic was also explained. Then, the structure of prototype for the verification of principle is explained. In this paper, the drive characteristics of the proposed motor by electromagnetic field analysis are predicted. As a result, it was possible to realize brushless secondary excitation by the second space harmonic, and it was confirmed that the torque generation could be improved. In the future works, set up the actual machine evaluation environment, verify the actual machine, and clarify the slip-torque characteristics and efficiency map etc. of the proposed brushless doubly-fed induction motor.

REFERENCES

- [1] V. Ostovic, "Memory Motors," IEEE Industry Applications Magazine, vol. 9, pp. 52–61, 2003.
- [2] K. Kato, N. Limsuwan, C. Y. Yu, K. Akatsu, and R. D. Lorenz, "Rare Earth Reduction Using a Novel Variable Magnetomotive Force, Flux Intensified IPM Machine," IEEE Trans. on IA., vol. 50, no.3, pp. 174801756, (May/June, 2016).
- [3] T. Nonaka, S. Oga, and M. Ohto, "Consideration about the Drive of Variable Magnetic Flux Motor," IEEJ Trans. on IA., vol. 135, no. 5, pp. 451-456, (2015) (in Japanese).
- [4] J. A. Tapia, F. Leonardi, and T. A. Lipo, "Consequent-Pole Permanent-Magnet Machine with Extended Field-Weakening Capability," IEEE Trans. on IA., vol. 39, no. 6, pp. 1704-1709, (1995).
- [5] M. Namba, K. Hiramoto, H. Nakai, "Novel Variable-Field Machine with a Three-Dimensional Magnetic Circuit," IEEE Trans. on IA., vol. 53, no. 4, pp. 3404-3410, (July/Aug., 2017).
- [6] T. Ogawa, T. Takahashi, M. Takemoto, H. Arita, A. Daikoku, and S. Ogasawara, "The Consequent-Pole Type Ferrite Magnet Axial Gap Motor with Field Winding for Traction Motor Used in EV," SAEJ Proc. of EVTeC & APE Japan 2016, no. 2169094, (2016).
- [7] A. Athavale, T. Fukushige, T. Kato, C. Y. Yu, and R. D. Lorenz, "Variable Leakage Flux (VLF) IPMSMs for Reduced Losses over a Driving Cycle while Maintaining the Feasibility, of High Frequency Injection-Based Rotor Position Self-Sensing," IEEE Energy Conversion Congress and Exposition 2014, (ECCE2014), (2014).
- [8] M. Minowa, H. Hijikata, K. Akatsu, and T. Kato, "Variable Leakage Flux Interior Permanent Magnet Synchronous Machine for Improving Efficiency on Duty Cycle," International Power Electronics Conference (IPEC-Hiroshima 2014 -ECCE ASIA-), (2014).
- [9] I. Urquhart, D. Tanaka, R. Owen, Z. Q. Zhu, J. B. Wang, and D. A. Stone, "Mechanically Actuated Variable Flux IPMSM for EV and HEV Applications," Proc. of EVS27 International Battery, Hybrid and Fuel Cell Vehicle Symposium 2013, pp. 0684-0695, (2013).
- [10] M. Aoyama, K. Nakajima, and T. Noguchi, "Proposal and Preliminary Experimental Verification of Electrically Reversal Magnetic Pole Type Variable Magnetic Flux PM Motor," IEEJ Journal of IA., vol. 7, no. 3, pp. 270-281, (2018).
- [11] M. Aoyama, and T. Noguchi, "Flux Intensifying PM-Motor with Variable Leakage Magnetic Flux Technique," The 2018 International Power Electronics Conference (IPEC-Niigata 2018 -ECCE ASIA-), pp. 718-725, (2018).
- [12] L. Yazhou, A. Mullane, G. Lightbody, and R. Yacmini, "Modeling of the Wind Turbine with a Doubly Fed Induction Generator for Grid Integration Studies," IEEE Trans. on Energy Conversion, vol. 21, no. 1, pp. 718-725257-264, (March, 2006).
- [13] S. Muller, M. Deicke, and R. W. De Doncker, "Doubly Fed Induction Generator Systems for Wind Turbines," IEEE Industry Applications Magazine, vol. 8, no. 3, pp. 26-33, (May/June 2002).
- [14] R. Li, R. Spee, A. K. Wallace, and G. C. Alexander, "Synchronous Drive Performance of Brushless Doubly-Fed Motors," IEEE Trans. on IA., no. 4, vol. 30, pp. 963-970, (1994).
- [15] B. V. Gorti, G. C. Alexander, and R. Spee, "Power Balance Considerations for Brushless Doubly-Fed Machines," IEEE Trans. on Energy Conversion, vol. 11, no. 4, pp. 687-692, (December, 1996).
- [16] O. Moros, J. Richnow, and D. Gerling, "New Cost Effective Concentrated Winding Topology for Induction Machines," ANSYS Conference & 32nd CADCAD User's Meeting 2014.
- [17] K. Yamazaki, N. Fukushima, "Iron Loss Model for Rotating Machines Using Direct Eddy Current Analysis in Electrical Steel Sheets," IEEE Trans. on Energy Conversion, vol. 25, no. 3, pp. 633-641, (2010).
- [18] I. Daut, K. Anayet, N. Gimesh, M. Asri, and Y. M. Irwan, "Comparison of Copper Rotor Bars with Aluminum Rotor Bars Using FEM Software -A Performance Evaluation-, 2009 Second International Conference on Computer and Electrical Engineering, vol. 1, pp. 456-459, (2009).
- [19] A. A. Jimoh, R. D. Findlay, and M. Poloujadoff, "Stray Losses in Induction Machines: Part II, Calculation and Reduction," IEEE Trans. on Power Apparatus and System, vol. PAS-104, no. 6, pp. 1506-1512, (1985).
- [20] M. Kondo, R. Ebizuka, and A. Yasunaga, "Rotor Design for High Efficiency Induction Motors for Railway Vehicle Traction," ICEMS2009, DSIG3-9, 2009.
- [21] H. A. Toliyat, T. A. Lipo, and J. C. White, "Analysis of a Concentrated Winding Induction Machine for Adjustable Speed Drive Applications," IEEE Trans. on Energy Conversion, vol. 6, no. 4, pp. 684-692, (1991).
- [22] M. Aoyama, and T. Noguchi, "Permanent-Magnet-Free Synchronous Motor with Self-Excited Wound-Field Technique Utilizing Space Harmonics," Applied Power Electronics Conference and Exposition (APEC), 2017 IEEE.